Seismic Damage Analysis of Zamora Bridge in Ecuador

Si Huang[1, a, *], and Zhan Chen [1, b]

[1] China Railway 14th Bureau Group Corporation Limited, Jinan 250101, China.

[a, *] 2495230130@qq.com , [b] 2245592599@qq.com

Abstract. The Zamora Bridge, located in the Zamora-Chinchipe Province in the southeastern part of Ecuador, on the Pacific Rim seismic belt, serves as the sole river-crossing channel from the Mirador Copper Mine area to the exterior. Constructed and opened for traffic in 2013, this bridge is designed as a low-pier continuous girder bridge, featuring a three-span prestressed concrete continuous box girder for the main beam, with a span arrangement of 45.5+140+45.5 meters, and utilizes basin-type rubber bearings throughout. On May 6, 2019, and November 28, 2021, the Zamora Bridge experienced two significant seismic events. The initial seismic damage investigation revealed that the piers and foundation maintained their load-bearing capacity largely intact; the basin-type rubber bearings predominantly suffered shear failure and displacement, losing their horizontal limit capacity. Additionally, abutment blocks sheared, padstones cracked locally, and the main girder exhibited residual displacement. Following the first earthquake, repair work was undertaken based on the damage results, switching to friction pendulum seismic isolation bearings to enhance the seismic resilience of bridge. The subsequent seismic damage assessment indicated the overall stable condition of the bridge, with no observable damage, deformation, or settling to the main structure, thus maintaining basic traffic functionality. However, shear and deformation occurred to the bolts and pins fixing the direction of the friction pendulum isolation bearings, along with residual displacements after the activation of the seismic isolation function, and cracks developed in the abutment padstones and mortar layers. To delve into the performance and damage probability of vulnerable components of low-pier continuous girder bridges under various seismic intensities, numerical models of the Zamora Bridge equipped with basin rubber bearings and friction pendulum bearings were separately established using OpenSees finite element software. An analysis of the bearings' longitudinal seismic susceptibility was conducted by integrating the demand-capacity ratio and IDA method. The findings indicate that bearings, padstones, and anchor bolts are the vulnerable components necessitating reinforcement for such bridges. Compared to the basin rubber bearings, friction pendulum bearings significantly reduce the probability of bearing damage and demonstrate an excellent seismic isolation effect.

Keywords: bridge engineering; seismic damage investigation; seismic vulnerability; demand-capacity ratio; IDA; OpenSees.

1. Introduction

With the continuous growth of China's economy, more and more roads are being built, gradually advancing from flat areas to undulating areas and from plane traffic to three-dimensional traffic. Restricted by terrain or surrounding architectural environment, short-pier bridges often appear. After investigating earthquake damage, it was found that short piers are more prone to shear failure. Housner [1] investigated the 1994 Northridge earthquake in the United States and found that 6 out of 7 collapsed bridges were caused by pier shear failure. In the 2008 Wenchuan earthquake in China, the short-pier rigid frame of the Huilan interchange bridge in Mianzhu City suffered severe flexural shear damage [2]. Shear failure of short piers is a brittle failure, and once it occurs, the bridge is very easy to collapse. The use of isolation bearings can effectively prolong the natural period of short-pier bridges, reduce the shear force on the piers, and protect the piers from shear failure. However, the vulnerability of various components of short-pier bridges with isolation bearings under earthquake action still needs further research.

The use of seismic vulnerability analysis to assess the seismic performance of bridges has been widely applied both domestically and internationally [3,5]. He et al. [6] employed the IDA dynamic analysis method and used the curvature of the critical section of the pier as a damage indicator to

perform seismic vulnerability analysis on railway hollow high-pier bridges. Wu et al. [7] established a finite element model for deep-water high-pier long-span bridges, and obtained key parameters such as the maximum stress and deformation of the structure by analyzing the seismic response of the bridge. On this basis, they conducted a seismic vulnerability assessment combining the PSI index. Shan et al. [8] used the incremental dynamic analysis method to input 3D seismic waves to study the impact of the horizontal seismic wave incidence angle on the exceedance probability of different levels of damage to bridge components. Bignell et al. [9] conducted a seismic vulnerability assessment of wall-pier-type highway bridges based on nonlinear pushover analysis. Bouazza et al. [10] used the incremental dynamic analysis method to study the correlation between steel slip, steel buckling, and low-cycle fatigue in the seismic vulnerability analysis of RC bridge piers.

2. Seismic Damage Investigation of the Zamora Bridge

2.1 First earthquake damage investigation

On May 26, 2019, at 2:41 AM local time, a strong earthquake with a magnitude of 8.0 struck northern Peru (5.85 degrees south latitude, 75.09 degrees west longitude), with an epicenter 490 km away and a focal depth of approximately 100 kilometers. The earthquake lasted about 3 minutes, affecting surrounding countries. This earthquake was the largest in Peru since 2007 and the strongest globally so far this year. The earthquake caused casualties in towns near the epicenter (according to incomplete statistics, at least one person died, and 11 were injured) and resulted in serious earthquake disasters, such as the collapse of more than 50 buildings and damage to some roads. During the earthquake, the Zamora Bridge area in Ecuador experienced strong shaking and a long duration, lasting about 3 minutes. The earthquake caused more severe earthquake disasters in the surrounding towns, such as cracks in some houses and landslides in the mountains.

The earthquake damage mainly includes shearing of the directional baffle in the bearing fixation direction, crushing of the padstones, partial fragmentation and spalling of the beam's corbel at the longitudinal movable bearing of pier 2, shearing of the anti-drop beam stop block bolts, and residual displacement of the beam. The specific damage is shown in Table 1.

Table 1. Damage status table of various components of the bridge

Location	Main Damage Conditions
main girder	Upon visual inspection, no damage was found, with no apparent deformation or cracks, and the linearity of the main girder remained unchanged. Partial damage occurred to the corbel on the right side at Pier 3, and the entire main girder shifted laterally by 2~5 cm and longitudinally by 5 cm. It is preliminarily assessed that the load-bearing capacity of the main girder has not significantly decreased.
piers and foundations	Visual inspection revealed no damage, no apparent deformation, settlement, or cracks, and the verticality remained unchanged. It is preliminarily assessed that the load-bearing capacity of the piers and foundations has not significantly decreased
bearings	Both the lateral and longitudinal fixed bearings experienced shear failure, with all bearings exhibiting a longitudinal displacement of 5 cm and a lateral displacement of 2~5 cm. It is preliminarily assessed that the horizontal limiting capacity of the bearings has failed, but the vertical load-bearing capacity has not significantly decreased.

padstones	Only the concrete of the padstones for the lateral fixed bearings at the abutments showed partial fragmentation and spalling, while the padstones for other bearings were mostly intact. It is preliminarily assessed that the load-bearing capacity of the damaged padstones at the abutments has decreased, and temporary protection and reinforcement should be considered for emergency traffic flow.
blocks	The seismic blocks for the multi-directional movable bearings at the abutments experienced shear failure, and the concrete seismic blocks at Pier 3 were partially damaged with diagonal cracks. It is preliminarily assessed that the damage to the seismic blocks at the middle pier is minor, and they can still provide some blocking and energy dissipation.
other ancillary structures	No damage was observed to the conical structures at the abutments, nor to the slope protection of the middle pier cap. However, some pedestrian railing foundations were damaged, some pedestrian walkway planks were warped, there was partial damage to the expansion joint steel, and the water stop strip had detached.

Analysis of Earthquake Damage Causes:

(1) Under the action of the earthquake, the horizontal shear force on the bearings exceeded their horizontal bearing capacity, causing shear damage to all longitudinal and lateral fixed bearings, leading to both longitudinal and lateral displacement of the beam.

(2) Deformation and shear damage to the bearing plate and bolts under the lateral fixed bearings at the abutment led to the fracturing of the surrounding concrete of the padstone.

(3) The lateral displacement of the beam caused the seismic blocks to impact the padstones, resulting in the damage of the seismic blocks at the abutment.

(4) The shearing of the bearings under the strong earthquake effectively dissipated the seismic forces, preventing more severe earthquake effects on the piers, foundations, and main girder. The main structure remained largely intact, with no apparent damage.

2.2 Second earthquake damage investigation

After the first earthquake, the Zamora Bridge was repaired based on the earthquake damage investigation results, including beam repositioning, partial repair of the main girder, repair of the padstones, and replacement of the bearing system. Considering that the bridge is located in the Pacific Ring of Fire, where strong earthquakes are frequent, the bearing system was replaced with friction pendulum isolation bearings in the repair plan.

On November 28, 2021, at 5:52 AM, a 7.5 magnitude earthquake occurred near the Ecuadorian border in Peru (4.490° S, 76.846° W), with an epicenter 250 km away. The mining area experienced strong shaking, and the earthquake lasted for about 2 minutes. The focal depth was 131 km, indicating a strong seismic activity in the mantle layer, with an intensity of VIII on the scale. The earthquake had a long duration and relatively large destructive potential. During this earthquake, the constraints of the friction pendulum isolation bearings were released, playing an isolation role. The main earthquake damage included shear pin and bolt shearing in the bearing stop plates, cracking of the abutment padstones, and residual displacement of the beam. The specific damage is shown in Table 2.

Table 2. Damage status table of various components of the bridge

Location	Main Damage Conditions

main girder	No damage was observed upon visual inspection, with no apparent deformation or cracks, and the overall linearity showed no significant change. The main girder at Pier 1 shifted left by 22mm, and at Pier 4, it shifted right by 11mm, with an overall longitudinal shift of about 3mm. It is assessed that the load-bearing capacity of the main girder has not significantly decreased.
piers and foundations	No damage was observed upon visual inspection, with no apparent deformation, settlement, or cracks, and no significant change in verticality. It is assessed that the load-bearing capacity of the piers and foundations has not significantly decreased.
bearings	Limit stop plate bolts for the lateral and longitudinal fixed bearings sheared off, with plates displaced or fallen off. The bearings played an isolation role, with a maximum residual displacement of about 22mm. The horizontal limit capacity of the bearings was released, but the vertical load-bearing capacity has not significantly decreased. Partial dowel holes on the seat plates under the lateral movable bearing and fixed bearing at Pier 3 deformed.
padstones	The maximum crack width on the padstone at Pier 1 was about 5mm, and Pier 4 experienced concrete splitting damage; minor cracks less than 1mm wide appeared on the padstones under the longitudinal movable bearing at Pier 2 and the fixed bearing at Pier 3. Other padstones were mostly intact. It is preliminarily assessed that the vertical load-bearing capacity of the padstones at the abutments has decreased, and temporary protection and reinforcement should be considered for emergency traffic flow.
blocks	No significant earthquake damage occurred to the seismic blocks.
other ancillary structures	The concrete on both sides of the expansion joints was intact, with no apparent cracks, but the rubber water stop in the middle of the expansion joint at Pier 4 was damaged. No uplift or cracks were found in the road foundations on both sides of the abutments.

Analysis of Earthquake Damage Causes:

(1) Under the action of the earthquake, the horizontal shear force on the bearings exceeded the horizontal bearing capacity of the limit stop plates, causing the release of the longitudinal and lateral fixed bearing constraints for the entire bridge, leading to both longitudinal and lateral displacement of the beam.

(2) The shear force in the fixed direction of the bearings caused cracking in the padstones of the abutment, the longitudinal movable padstone of Pier 2, and the fixed padstone of Pier 3.

(3) Due to the release of the fixed-direction constraints of the bearings under the earthquake action, the isolation function was activated, effectively reducing the seismic forces and preventing more severe earthquake effects on the piers, foundations, and main girder. The main structure remained intact, with no apparent damage.

3. Vulnerability Analysis Process and Selection of Seismic Motion

3.1 Vulnerability Analysis

3.1.1 Demand-Capacity Ratio Model

At a certain damage state, the ratio of seismic demand to structural capacity is defined as the damage index. Linear quadratic regression fitting is performed for the logarithm of damage index and the logarithm of peak ground acceleration, obtaining the mean (μ) and standard deviation (σ). The vulnerability function is:

$$P_f = P\left[\frac{S_d}{S_c} \geq 1\right] = 1 - \varphi\left(\frac{\ln(1) - \lambda}{\sigma}\right) = \varphi\left(\frac{\lambda}{\sigma}\right) \tag{1}$$

$$\lambda = a\ln(PGA)) + b \tag{2}$$

$$\sigma = \sqrt{S_r / (n-2)} \tag{3}$$

In the equation, a and b are the regression statistical analysis parameters; Sr is the sum of squared residuals of each discrete point relative to the regression curve; n is the number of discrete points.

3.1.2 Analysis Process

(1) Collect basic information about the bridge: including site conditions, structural type, construction records, etc.

(2) Select appropriate earthquake waves based on the geographic location and structural type of the bridge, and determine the intensity parameters of the earthquake waves. According to the basic information of the bridge, determine the damage indices of each component and the damage threshold values under different damage states.

(3) Choose peak ground acceleration (PGA) as the seismic intensity parameter. Adjust the intensity of the earthquake waves using a set of amplitude modulation coefficients to obtain earthquake wave records with PGAs ranging from 0.05g to 1.0g, with an increment of 0.05g.

(4) Determine the uncertainty parameters of the bridge structure. Use Latin hypercube sampling to extract parameter samples and establish finite element models based on the extracted parameter samples. Randomly combine the finite element models of earthquake waves and different parameter samples to perform a series of nonlinear time-history analyses, obtaining the seismic demand response of the structure. Then, calculate the ratios of seismic demand response to different damage indices.

(5) Perform logarithmic regression analysis on the demand-capacity ratio and PGA to obtain the regression mean and standard deviation of the demand-capacity ratio, as shown in equations (2) and (3). Then, use equation (1) to calculate the damage exceedance probability of the structure under different levels of seismic intensity. Based on the calculated results, plot the seismic vulnerability curves of bridge components such as piers and bearings.

3.2 Ground motion selection

Seismic input generally includes two aspects: the first is the seismic intensity parameters, such as seismic intensity, peak ground acceleration (PGA), and seismic period; the second is the seismic wave time history, which is the time-varying curve of seismic motion, reflecting the complexity and irregularity of the seismic motion. Ten earthquake motion records that meet the site requirements of the bridge location are selected from the strong motion database of the Pacific Earthquake Engineering Research Center (PEER) in the United States. The epicentral distances of the selected earthquakes are all greater than 30 km, excluding the influence of near-field pulse-type earthquakes on the structural response. The 10 selected ground motion parameters are shown in Table 3.

Table 3. Earthquake parameters table

Number	Name	Station	M_w	R_{jb}/km	PGA/g
1	Kobe Japan	Tadoka	6.9	28.28	0.152
2	Kocaeli Turkey	Delta	7.51	31.74	0.137
3	Imperial Valley-06	Holtville Post Office	6.53	22.03	0.235
4	Darfield New Zealand	Kaiapoi North School	7.0	30.53	0.360
5	Cape Mendocino	College of the Redwoods	7.01	29.22	0.141
6	Northridge-01	Alhambra-Fremont School	6.69	35.66	0.100
7	Chi-Chi Taiwan-04"	CHY088	7.62	37.48	0.212
8	Loma Prieta	Halls Valley	6.93	30.25	0.134
9	Landers	Indio-Jackson Road	7.28	48.84	0.307
10	Tabas_ Iran	Boshrooyeh	7.35	24.07	0.105

4. Bridge Introduction and Modeling

4.1 Bridge Specifications

The Zamora Bridge starts at kilometer marker K6+383.043 and ends at K6+626.543, with a total length of 243.5 m. The schematic diagram of the bridge structure is shown in Figure 1. The bridge adopts a three-span prestressed concrete continuous box girder structure with calculated spans of 45.5+140+45.5 m. The bottom edge of the mid-span beam follows a quadratic parabolic variation, while the bottom edge of the side-span beams follows a linear variation. The distance from the centerline of the side bearings to both ends is 0.6 m.

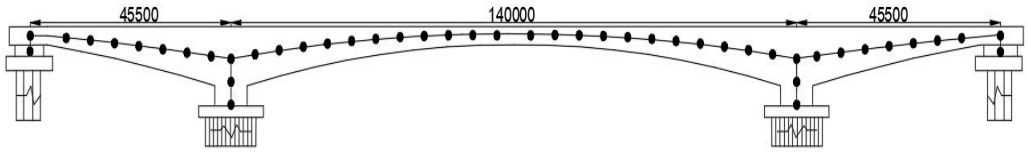

Fig. 1 Bridge structure diagram

4.2 Three-dimensional modeling of the bridge structure

A finite element dynamic analysis model of the continuous beam bridge is established using OpenSees. In the seismic design of bridges, the upper structure of the bridge is usually required to remain elastic during an earthquake to ensure the stability and reliability of the structure. Actual earthquake damage data also indicate that the upper structure of the bridge generally does not suffer significant damage. Therefore, elastic beam elements are used to simulate the response of the upper structure. In this project, the bridge piers are short piers, which, according to post-earthquake survey data, are prone to shear failure. To more accurately consider the impact of shear forces on the piers, the Timoshenko beam-column elements are used to simulate the piers. The pile foundation is simulated using equivalent boundary elements. The equivalent stiffness of the soil-pile spring is calculated using the m-method, based on the engineering survey, test data, and parameter recommendations related to soil layers, combined with the distribution map of soil layers for the bridge. Bearings are simulated using zero-length elements, requiring the definition of stiffness in six degrees of freedom. The horizontal stiffness uses the Steel01 material to simulate the elastoplastic

behavior of the bearings, while the vertical stiffness is generally taken as a larger value. The torsional stiffness is generally not considered and is treated with a smaller value.

5. Seismic Vulnerability Analysis of the Zamora Bridge

5.1 Adopting basin type rubber bearings

5.1.1 Damage indicators

The earthquake damage investigation found that bearings and padstones are prone to damage under seismic action. Limited by the length of this article, only the vulnerability analysis of the bearings is conducted. Figure 2 shows the arrangement of basin-type rubber bearings. The relative displacement between the upper and lower ends of the bearing is used as the damage index, and the damage index thresholds for basin-type rubber bearings are obtained, as shown in Table 4 and 5.

Fig. 2 Arrangement of basin-type rubber bearings

Table 4. 2# movable basin bearing damage indicators

Damage Level	Relative Displacement/mm
no damage	$d<37$
minor damage	$37\leq d<75$
moderate damage	$75\leq d<112$
severe damage	$112\leq d<150$
complete damage	$d\geq 150$

Table 5. 6# movable basin bearing damage indicators

Damage Level	Relative Displacement /mm
no damage	$d<25$
minor damage	$25\leq d<50$
moderate damage	$50\leq d<75$
severe damage	$75\leq d<100$
complete damage	$d\geq 100$

5.1.2 Result analysis

Statistical analysis is performed on the maximum relative displacement of the basin-type rubber bearings under each earthquake motion. Logarithmic regression fitting is conducted on the maximum displacement demand-capacity ratio of the bearings and seismic parameters to obtain the regression fitting function for minor damage to the bearings. Based on Equation (1) and the logarithmic regression fitting, the exceedance probabilities for each damage state are calculated. From this, the vulnerability curves for the bearings are drawn. Figure 3 shows a comparison of the longitudinal seismic vulnerability curves for bearings #2 and #6.

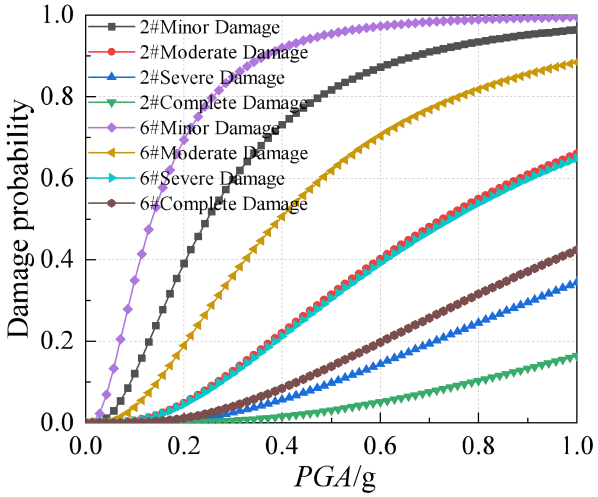

Fig. 3 Longitudinal seismic vulnerability curves of 2# and 6# basin rubber bearings

As shown in Figure 3, the damage exceedance probability of the basin-type rubber bearings increases with the intensity of seismic motion. The damage trends of bearings #2 and #6 are basically the same, but the damage exceedance probability of bearing #6 is greater than that of bearing #2. When the peak ground acceleration (PGA) is around 0.15g, the exceedance probability of minor damage for bearing #6 is 50%, and when the PGA is around 0.25g, the exceedance probability of minor damage for bearing #2 is 50%. At 1.0g, the probability of minor damage for both bearings is approaching 100%. The exceedance probability of severe damage for bearing #2 is around 35% at 1.0g, while for bearing #6, it is around 65%. The exceedance probability of complete damage for bearing #2 does not exceed 20% at 1.0g, while for bearing #6, it does not exceed 50%. It can be seen that when using basin-type rubber bearings, the probability of damage to the bearings under seismic action is relatively high, and it is necessary to replace them with isolation bearings to improve the seismic performance of the bridge.

5.2 Adopting friction pendulum bearings

5.2.1 Damage indicators

Figure 4 shows the arrangement of friction pendulum bearings. The seismic design displacement Dd of the friction pendulum bearing is 200 mm, and the radius R is 4000mm. The design displacement of the bearing is used as the threshold value for minor damage, and Dd2=0.2R=800 mm is used as the threshold value for complete damage. The damage states of the friction pendulum bearing are divided into five levels, with each level and its damage index shown in Table 6.

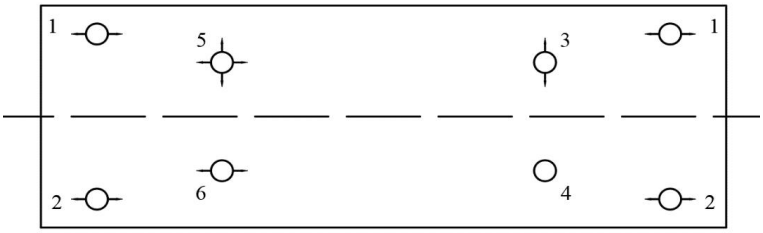

Fig. 4 Arrangement of friction pendulum bearings

Table 6. Friction pendulum bearing damage indicators

Damage Level	Relative Displacement /mm
no damage	$D \leq 200$
minor damage	$200 < D \leq 300$
moderate damage	$300 < D \leq 500$

severe damage	$500<D\leq800$
complete damage	$D>800$

5.2.2 Result analysis

The maximum relative displacement of the friction pendulum bearings under each earthquake motion is recorded, and the vulnerability curves of the friction pendulum bearings are drawn using the method mentioned above. Figure 5 shows a comparison of the longitudinal seismic vulnerability curves for bearings #2 and #6.

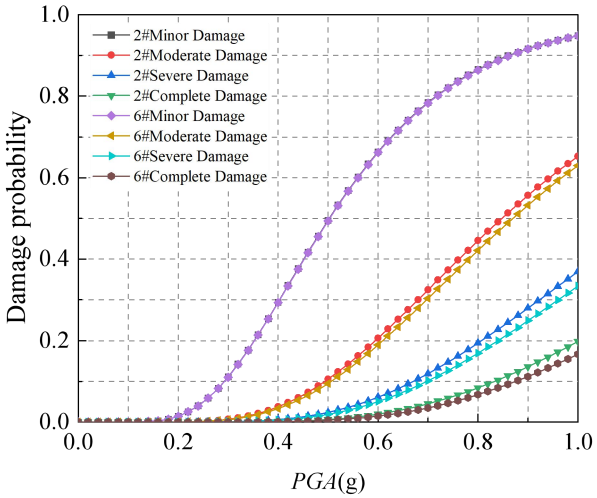

Fig. 5 Longitudinal seismic vulnerability curves of 2# and 6# friction pendulum bearings

From Figure 5, it can be seen that the vulnerability curves for minor damage to bearings #2 and #6 with friction pendulum bearings almost completely overlap, while for other degrees of damage, the probability of damage to bearing #2 is slightly greater than that of bearing #6. When the peak ground acceleration (PGA) is around 0.5g, the exceedance probability of minor damage for bearings #2 and #6 is around 50%, and at 1.0g, the probability of minor damage to the bearings is approaching 100%. The exceedance probability of severe damage to the bearings does not exceed 50% at 1.0g, and the exceedance probability of complete damage does not exceed 20% at 1.0g. The use of friction pendulum bearings has reduced the seismic response of the structure and significantly decreased the probability of damage to the bearings.

6. Summary

This paper compares two earthquake damage investigations of the Zamora Bridge in Ecuador, and establishes a finite element model by OpenSees. The seismic vulnerability analysis of the Zamora Bridge with basin-type rubber bearings and friction pendulum bearings is conducted using the demand-capacity ratio and IDA methods, yielding the following conclusions:

(1) The two earthquake damage investigations indicate that bearings, padstones, and anchor bolts are vulnerable components. It is necessary to reinforce these components for this type of bridge.

(2) When using two different types of bearings, the damage exceedance probabilities of bearings #2 and #6 are inconsistent. For basin-type rubber bearings, the damage exceedance probability of bearing #6 is greater than that of bearing #2. For friction pendulum bearings, the probability of damage to bearing #2 is slightly higher than that of bearing #6, but the difference is not significant.

(3) The exceedance probabilities of all damage levels for the friction pendulum bearings in the longitudinal direction are generally lower than those for the basin-type rubber bearings. This indicates that friction pendulum bearings have good seismic isolation effects, and the use of isolation bearings can effectively reduce the probability of damage to the bearings.

References

[1] Housner G W, Thlel C C. The continuing challenge:report on the performance of state bridges in the north ridge earthquake. Earthquake Spectra, 1995, 1(4): 607-636.

[2] Sun Zhiguo, Wang Dongsheng, Guo Xu, et al. Damage investigation of Huilan Inter change in Mianzhu after Wenchuan earthquake. Journal of Earthquake Engineering and Engineering Vibration, 2009, 29(4): 132-138.

[3] Cornell C A, Jalayer F, Hamburger R O, et al. Probabilistic Basis for 2000 SAC Federal Emergency Management Agency Steel Moment Frame Guidelines. Journal of Structural Engineering, 2002, 128(04): 526-533.

[4] Jiang Wei. Fragility analysis of RC-Continuous highway bridge. Huazhong University of Science and Technology, 2012.

[5] Marco G, Romeo T, Emidio N. The soil-structure interaction effect on the seismic vulnerability assessment and retrofitting of existing bridges. Procedia Structural Integrity, 2023, 44: 618-625.

[6] He Chuankai, Chen Jing. Seismic fragility analysis of hollow high-pier railway-bridge. Earthquake Resistant Engineering and Retrofitting, 2021, 43(03): 32-39.

[7] Wu Wenpeng, Liang Peng, Long Shiguo et al. Seismic fragility analysis for high-pier and long-span bridges in deep water considering pile-soil interaction. Journal of Vibration and Shock, 2020, 39 (19): 210-217.

[8] Shan Deshan, Han Lulu,Qu Faxian, et al. Impact of ground motion incident angles on seismic vulnerability for bridge with thin-walled hollow tall pier. Journal of Traffic and Transportation Engineering, 2020, 20(06): 90-103.

[9] Bignell J L ,Lafave J M ,Hawkins N M . Seismic vulnerability assessment of wall pier supported highway bridges using nonlinear pushover analyses. Engineering Structures, 2005, 27(14): 2044-2063.

[10] Bouazza H, Djelil M, Matallah M. On the relevance of incorporating bar slip, bar buckling and low-cycle fatigue effects in seismic fragility assessment of RC bridge piers. Engineering Structures, 2022, 256: 114032.